Optimal Design of High-Order Passive-Damped Filters for Grid-Connected Applications

Beres, Remus Narcis; Wang, Xiongfei; Blaabjerg, Frede; Liserre, Marco; Bak, Claus Leth

Optimal Design of High-Order Passive-Damped Filters for Grid-Connected Applications

Remus Narcis Beres, *Student Member, IEEE*, Xiongfei Wang, *Member, IEEE*, Frede Blaabjerg, *Fellow, IEEE*, Marco Liserre, *Fellow, IEEE*, and Claus Leth Bak, *Senior Member, IEEE*

Abstract—Harmonic stability problems caused by the resonance of high-order filters in power electronic systems are ever increasing. The use of passive damping does provide a robust solution to address these issues, but at the price of reduced efficiency due to the presence of additional passive components. Hence, a new method is proposed in this paper to optimally design the passive damping circuit for the *LCL* filters and *LCL* with multituned *LC* traps. In short, the optimization problem reduces to the proper choice of the multisplit capacitors or inductors in the high-order filter. Compared to existing design procedures, the proposed method simplifies the iterative design of the overall filter while ensuring the minimum resonance peak with a lower damping capacitor and a lower rated resistor. It is shown that there is only one optimal value of the damping resistor or quality factor to achieve a minimum filter resonance. The passive filters are designed, built, and validated both analytically and experimentally for verification.

Index Terms—Harmonic passive filters, *LCL* filter, resonance damping, *trap* filter, voltage-source converters.

I. INTRODUCTION

THE introduction of high-order filters to limit out the switching harmonics from grid-connected voltage-source converters (VSC) is associated with improved attenuation performance and consequently decrease in size, volume, and cost of the filter [1]. An example of such high-order filter is the *LCL* filter, which became well accepted and widely used as an interface between renewable energy sources and the utility grid [1]–[7]. The use of harmonic *LC traps* instead of the *LCL* filter capacitor gains interests from industry, due to the possibility to reduce or even eliminate the grid-side filter inductor [8]. In [9], the *trap* filter was proposed for single-phase grid-connected converters under the name of *LLCL* filter, but with a small inductance on the grid side of the filter. It was further shown in [10] that the size and volume of the filter can theoretically be reduced by adopting up to three multituned *traps*.

However, the resonances that arise among the reactive elements of the high-order filters may require a damping circuit in order to avoid instabilities in the current controller of the grid converters. It has recently been shown that no damping

is required for the grid current control, if the *LCL* filter resonance frequency is higher than the critical resonance frequency, which is one-sixth of the control frequency [11]. If the converter current is controlled, then, opposite result is obtained [12]. However, the stability condition of the power converter is also largely dependent on the grid impedance [13]. Under the unknown grid impedance condition (equivalent to a grid dominated by power electronics systems), damping may be necessary to attenuate the filter resonance and mitigate the oscillatory behavior of the converter-based system connected to the utility grid [14]. To reduce the filter resonances, both active and passive damping can be used [15]. Adopting different active damping methods, an increased number of sensors may be required and the robustness of the filter may not be ensured, especially due to the sensitivity toward filter parameters/grid impedance variations [15]. On the other hand, if a passive resistor is placed in series with the filter capacitor, the damping becomes more robust and the stability of the filter is always improved, but at the price of increased losses and decreased high-frequency attenuation [4].

In general, passive damping losses can be reduced by using additional reactive components in the filter circuit. Several topologies for damping the *LCL* filter resonance have recently been reviewed in [16], [17]. However, there is a lack of applicable guidelines on how to optimally design those damping circuits. For the *LLCL* filter, some damping methods were investigated in [18] together with a new method to optimally design the damping elements. However, the procedure formulated in [18] cannot directly be used to derive the optimal parameters of the filter, and many iterations are required to meet the design requirements for the filter. Similarly, an optimization procedure was proposed in [19] for the *LCL* filter, but the adopted damping resistor is fixed in value even the damping circuit ratings changes. This may translate to an inefficient use of the damping circuit. Additionally, the reader may have no insight about how to design the damping circuit. A detailed optimal damping design procedure of an *LC* filter used for dc–dc converters was proposed by Middlebrook in [20] and extended by Erickson in [21]. It was clearly shown how to design the damping circuit for a *LC* filter, i.e., the exact value of the damping resistor, the actual resonance of the filter when a passive damping circuit is used or the filter quality factor. For the passive damping of the *LCL* or *trap* filters, none of the practical considerations given in [20], [21] are yet available for the filter designer, and a trial-error tuning procedure is typically adopted. Therefore, in this paper the Middlebrook design method is extended to high-order filters employed in ac grid-connected applications. Compared to the existing design procedures, the proposed method simplifies the

Fig. 1. Simplified diagram of a three-phase grid-interfaced VSC with high-order filter.
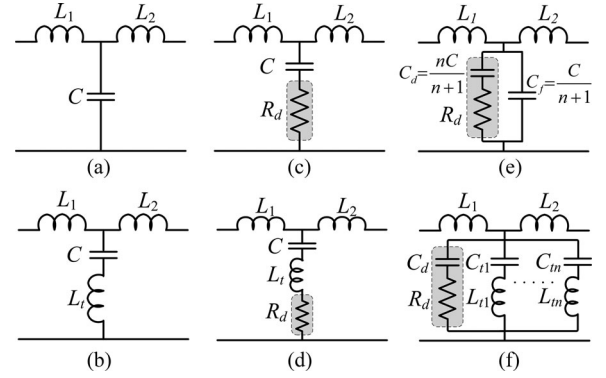

Fig. 2. Simplified one-line schematic of high-order filters: (a) *LCL* filter. (b) *Trap* filter. (c) *LCL* filter with series damping resistor. (d) *Trap* filter with series damping resistor. (e) *LCL* filter with shunt *RC* damper. (f) Multituned *traps* filter with shunt *RC* damper.

iterative design procedure of the overall filter, while ensuring a minimum resonance peak, a smaller damping capacitor, and a lower rated damping resistor. For verification, three power filters prototypes are designed and validated both analytically and experimentally.

The paper is organized as follows. An overview of the passive filters characteristics is presented first, from which the main design constraints of the filters are systematically identified. The proposed optimal damping design procedure is discussed afterward. An overall filter design for the proposed filters is formulated before the demonstration on a laboratory prototype. The main findings conclude the paper.

II. GRID-INTERFACED VSC WITH HIGH-ORDER FILTERS

A. State Space Model

A generic high-order filter schematics is shown in Fig. 1 on a per phase basis. Based on the notations given in Fig. 1, the state-space model of such a circuit can be built considering the converter side voltage V_1 and the grid voltage V_2 as the input variables [7]. The output variables can then be the converter current I_1 and the grid current I_2 depending on which of them is to be controlled. The state space equations can be written as

$$\begin{bmatrix} I_1 \\ I_2 \end{bmatrix} = - \begin{bmatrix} Y_{11} \\ Y_{21} \end{bmatrix} V_1 - \begin{bmatrix} Y_{12} \\ Y_{22} \end{bmatrix} V_2 \qquad (1)$$

where Y_{11} denotes the filter input admittance, Y_{12} the filter reverse trans-admittance, Y_{21} the filter forward trans-admittance, and Y_{22} the filter output admittance.

For example, if the grid current is the control variable, then the current control open loop can be written as

$$Y_{\mathrm{ol}}(s) = G_{PR}(s) G_{\mathrm{Delay}}(s) Y_{21}(s) \qquad (2)$$

where the forward transadmittance of the filter (Y_{21}) is the current controller plant, G_{PR} is a proportional-resonant (*PR*) current regulator responsible to generate the reference voltage for the pulse width modulator (*PWM*), and G_{Delay} denotes the delay due to digital computation. Equation (2) implies a pure sinusoidal grid voltage. If background voltages exist in the grid, then the grid voltage and the filter output admittance (Y_{22}) must be considered accordingly in (2) as disturbance. The analysis hereafter is done considering only the grid current feedback, in addition to an ideal grid voltage. It is expected that background voltage if exists, do not influence the analysis since the resonance of the filter adopted later in this paper is significantly higher than typical low-order harmonics found in the grid. If

the converter current is used for the feedback control then Y_{21} should be replaced with Y_{11} in (2). The forward transadmittance transfer function of a high-order filter can be generalized as

$$Y_{21} = \left. \frac{I_2}{V_1} \right|_{V_2=0} = \frac{Z_{3f}}{Z_{1f} Z_2 + Z_{1f} Z_{3f} + Z_2 Z_{3f}} \qquad (3)$$

where Z_{1f} denotes the converter side impedance of the filter, $Z_2 = Z_{2f} + Z_{2g}$ is the impedance on the grid side of the filter which consist of the filter grid side impedance Z_{2f}, and the impedance of the grid Z_{2g}; Z_{3f} denotes the impedance of the filter in the parallel branch. Y_{21} can be used to evaluate the harmonic attenuation performance of the filter, i.e., indicates how the harmonic voltages specific to a given modulation strategy propagates into the grid current.

B. Derivation of Passive Filters Transfer Functions

The one-line schematics of several high-order filters are illustrated in Fig. 2, with the equivalent series resistances (*ESR*) of the filter components neglected for simplicity. In practice, the ESR of typical inductive components will slightly increase the damping effect in the system, with the effect being more dominant at higher frequencies because of the skin effect. Additionally, L_2 accounts all the equivalent inductances of the actual grid and the filter. In Fig. 2(e) and (f), the sum of the multisplit capacitors is chosen equal with the capacitance of the *LCL* filter, i.e., the capacitance in the filter is fixed to a given value. More explanations will be covered in the forthcoming section.

For the *LCL* filter, the filter forward transadmittance may be written as

$$Y_{21(LCL)}(s) = \left. \frac{I_2(s)}{V_1(s)} \right|_{V_2=0} = Y_0 \frac{1}{\frac{s^2}{\omega_0^2} + 1} \qquad (4)$$

$$Y_{21(LCL)}(s) = Y_\infty \frac{1}{\frac{\omega_0^2}{s^2} + 1}. \qquad (5)$$

The corresponding low-frequency asymptote Y_0, high-frequency asymptote Y_∞, and the characteristic resonant pole frequency ω_0 of the filter are expressed in Table I. The inverted poles arrangement in (5) reveals the *LCL* filter attenuation

TABLE I
MAIN COEFFICIENTS AND FEATURES OF THE FILTER TRANSFER FUNCTIONS

Filter topologies	Y_0	Y_∞	$R_0 (Q = R_d/R_0)$	ω_0	ω_t
LCL	$[s(L_1 + L_2)]^{-1}$	$(s^3 L_1 L_2 C)^{-1}$	$\sqrt{L/C}$	$(\sqrt{LC})^{-1}$	–
LCL + R	$[s(L_1 + L_2)]^{-1}$	$R_d / (s^2 L_1 L_2)$	$\sqrt{L/C}$	$(\sqrt{LC})^{-1}$	–
LCL + RC	$[s(L_1 + L_2)]^{-1}$	$(n+1)/(s^3 L_1 L_2 C)$	$\sqrt{L/C}$	$(\sqrt{LC})^{-1}$	–
Trap	$[s(L_1 + L_2)]^{-1}$	$L_t / [s(L_1 L_2 + L_1 L_t + L_2 L_t)]$	$\sqrt{(L+L_t)/C}$	$(\sqrt{(L+L_t)C})^{-1}$	$(\sqrt{L_t C})^{-1}$
Trap + R	$[s(L_1 + L_2)]^{-1}$	$L_t / [s(L_1 L_2 + L_1 L_t + L_2 L_t)]$	$\sqrt{(L+L_t)/C}$	$(\sqrt{(L+L_t)C})^{-1}$	$(\sqrt{L_t C})^{-1}$
Trap + RC	$[s(L_1 + L_2)]^{-1}$	$R_d / (s^2 L_1 L_2)$	$\sqrt{(L+L_t)/C}$	$(\sqrt{(L+L_t)C})^{-1}$	$(\sqrt{L_t C})^{-1}$

above the characteristic frequency ω_0. From (5), two design constraints of the filters need to be considered. The first constraint refers to the placement of the characteristic frequency, which should be far away from the dominant harmonics of the grid background voltage. The second constraint denotes the high-frequency asymptote, which should ensure proper attenuation of the switching harmonics generated from the VSC, according to applicable harmonic standards.

For the *trap* filter, an additional inductor L_t is connected in series with the filter capacitor, as shown in Fig. 2(b). The additional inductor with the filter capacitor provides a notch characteristic around the switching frequency of the VSC. In this case, the forward transadmittance transfer function of the filter contains an additional conjugate zero pair ω_t

$$Y_{21(Trap)} = Y_0 \frac{\frac{s^2}{\omega_t^2} + 1}{\frac{s^2}{\omega_0^2} + 1}. \tag{6}$$

The inverted pole transfer function is omitted for simplicity. However, the corresponding high-frequency asymptotes are indicated in Table I. For the *trap* filter, an additional design constraint result in the choice of the notch frequency and corresponding notch parameters.

The consequent resonance of the filters can reduce the range of the current regulator gain and oscillatory behavior can occur. Since the resonance frequency of the filter shifts with changes in the grid impedance or drifts in the filter parameters, the resonance problem may become a difficult task to handle. A simple solution to ensure the stability of the VSC is to dampen the filter resonance by placing a resistor in series with the filter capacitor, as shown in Fig. 2(c) and (d). Considering the additional damping element, (4) and (6) can be written as

$$Y_{21(LCL+R)}(s) = Y_0 \frac{\frac{Qs}{\omega_0} + 1}{\frac{s^2}{\omega_0^2} + \frac{Qs}{\omega_0} + 1} \tag{7}$$

$$Y_{21(Trap+R)} = Y_0 \frac{\frac{s^2}{\omega_t^2} + \frac{Q}{\omega_0}s + 1}{\frac{s^2}{\omega_0^2} + \frac{Q}{\omega_0}s + 1}. \tag{8}$$

The series damping resistor in (7) and (8) adds a single zero given mainly by the quality factor Q of the filters. Another constraint in the filter design is represented by the quality factor, which should be designed in such way to limit the filter resonance influence in the controller system and to attain a good

dynamic response of the VSC current control. For stability purposes, both the phase and gain of the open loop current control should be taken into account. There is also a physical limit in dampening the filter resonance, given by the power loss in the damping resistor which is dependent mainly on the value of the percentage capacitor. With larger percentage capacitor, the fundamental and harmonic current in the damping resistor will result also larger. Additional cooling may be required in such cases which in turn will increase the size and cost of the system and reduce the efficiency [22].

A shunt damping resistance R_d in series with a blocking capacitor C_d can be employed to reduce the damping losses and to increase the high-frequency attenuation of the filter. Such benefits can be obtained due to the fact that damping is more selective if an *RC* damper is adopted as it acts only around the resonance frequency of the filter (more information in the next section). Therefore, this damping solution can be more effective than the conventional series resistor case [20], [23]. The shunt *RC* damper used with the *LCL* and multituned *traps* filters is illustrated in Fig. 2(e) and (f). In the case of the *trap* filter, several multituned traps can theoretically be employed to further reduce the size of the filter. However, in practice, the number of traps is limited up to three because of the very large impedance of the filter at multiples of the switching frequency [10]. The additional design problem for this type of damping will then be the proper choice of the ratio between the filter and the damping capacitor, i.e., how the filter total capacitance should be split between the different parallel branches in the filter. If only one trap is to be employed, then the transfer functions of the *LCL* and *trap* filters with the shunt *RC* damper becomes

$$Y_{21(LCL+RC)} = Y_0 \frac{\frac{nQ}{n+1}\frac{s}{\omega_0} + 1}{\frac{nQs^3}{(n+1)^2 \omega_0^3} + \frac{s^2}{\omega_0^2} + \frac{nQ}{n+1}\frac{s}{\omega_0} + 1}. \tag{9}$$

Compared with (7) and (8), additional poles and zeros are included in (9) and (10) as shown at the bottom of the next page which make more difficult the selection of the filter parameters.

C. High-Order Passive Filters Comparison

The main characteristics of the passive filters illustrated in Fig. 2 can be identified from Table I, where $L = L_1 L_2/(L_1 + L_2)$. In (10), an inductance factor $a = L_t/L$ is introduced to simplify the transfer function. The attenuation of the filters at

low and high frequencies can be found from the superscript of the Laplace operator of the low- and high-frequency asymptotes, Y_0 and Y_∞, respectively. Therefore, below the characteristic frequency, the filters exhibit the same inductive behavior, given by the sum of the converter and grid side inductances. In case of the *LCL* filter, the high-frequency harmonics are attenuated with a slope of 60 dB/decade. Adding the series damping resistor, the attenuation is reduced by 20 dB/decade. With the shunt *RC* damper, the high-frequency attenuation slope is not reduced, but is shifted by a factor of $(n + 1)^{-1}$. In case of the *trap* filter, above the tuned frequency the high-frequency harmonics are attenuated with a slope of only 20 dB/decade. However, the drawback of reduced attenuation at high frequencies is compensated by the fact that the attenuation of the most dominant harmonics (around the switching frequency) is theoretically infinite. By potentially downsizing the filter components accordingly, the size and volume of the overall filter can be reduced even more compared with the *LCL* filter [9], [10]. The series damping resistor only reduce the attenuation around the characteristic frequency and tuned frequency; therefore, the low- and high-frequency behavior of the filter is identical with the undamped *trap* filter. The shunt *RC* damper in a *trap* filter provides the advantage of increasing the high-frequency attenuation slope to 40 dB/decade. However, an additional resonance peak at a frequency higher than the tuned frequency is an additional design constraint which should be carefully taken into consideration [24]. In order to demonstrate the preliminary analysis of the filters, the magnitude plots of each of the calculated filter forward transadmittances are illustrated in Fig. 3, assuming same ratings for the passive components.

III. OPTIMIZED PASSIVE DAMPING DESIGN

A. Passive Damping Design Considerations

The design of the *LCL* filter is covered in detail in [1], [5] and [6] while of the *trap* filter is discussed in [8] and [9]. Hence, the optimization of the passive damping circuit and its influence on the *LCL* and *trap* filter parameters is considered hereafter. When passive damping is adopted, several compromises must be faced by the filter designer.

1) Peak in the Filter Admittance and the Actual Value of the Filter Resonance Frequency: Since the peak of the filter admittance around the resonance frequency limit the range of the current regulator gain, it is important to limit the filter admittance peak in order to avoid possible oscillatory behavior in the control system. The problem is that with any kind of damping in the system, the actual resonance of the filter is different from the characteristic frequency defined in the previous section. Additionally, the frequency shift will largely depend on the actual ratings of the filter components and the grid impedance condition. Typical factors in low-voltage applications that affect the
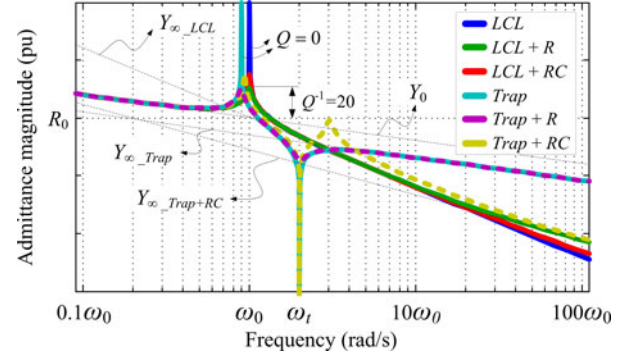

Fig. 3. Generalized admittance magnitude of the passive filters based on (5)–(10), given same L_1, L_2, C; $\omega_t = 2\omega_0$ and in case of passive damping, $Q = 0.05$ and $n = 1$.

control stability and require the limitation of the peak in the filter admittance may include:

1) up to 70% decrease in the filter inductance due to permeability dependence of the magnetic material with the magnetic field strength;
2) up to $\pm 30\%$ tolerances in the passive components;
3) wide range variation of the equivalent grid inductance: 0.3–2.5 mH.

Therefore, the choice of the damping circuit ratings should ensure the stability of the current controller for the intended operating range conditions.

2) Optimal Choice of the Damping Circuit Ratings Without Impairing Other Features of The Filter: Typically, the use of passive damping improve the stability in the control system but at the price of increased inefficiency of the overall system due to increased power loss, increased size of the filter, etc.

In the following, the optimized passive damping design method extended from [20] is demonstrated for the *RC* damper shunt illustrated in Fig. 2(e) and (f), but can equally be derived for other passive damping topologies, like presented in [16] and [21], i.e., filter topologies that uses multisplit capacitors or inductors in addition to the damping resistor.

B. Shunt RC Damper for LCL Filters

The main advantage of the *RC* damper shunt is the selective attenuation of the filter resonance. In Fig. 4 is illustrated the characteristic of the parallel branch impedance of the *LCL* filter with *RC* damper shunt. It can be seen that at lower frequencies and higher frequencies, the impedance of the damper is capacitive. Therefore, it provides two main benefits over the series damping resistor solution. On one hand, the slope of the high-frequency attenuation of the filter is maintained at 60 dB/decade. The other advantage is the power loss reduction in the resistor since the current is split between the two capacitors. The corner

$$Y_{21(Trap+RC)} = Y_0 \frac{\frac{anQs^3}{(a+1)(n+1)^2\omega_0^3} + \frac{as^2}{(a+1)(n+1)\omega_0^2} + \frac{nQs}{(n+1)\omega_0} + 1}{\frac{ans^4}{(a+1)^2(n+1)^2\omega_0^4} + \frac{nQs^3}{(n+1)^2\omega_0^3} + \frac{(a+n+1)s^2}{(a+1)(n+1)\omega_0^2} + \frac{nQs}{(n+1)\omega_0} + 1} \tag{10}$$
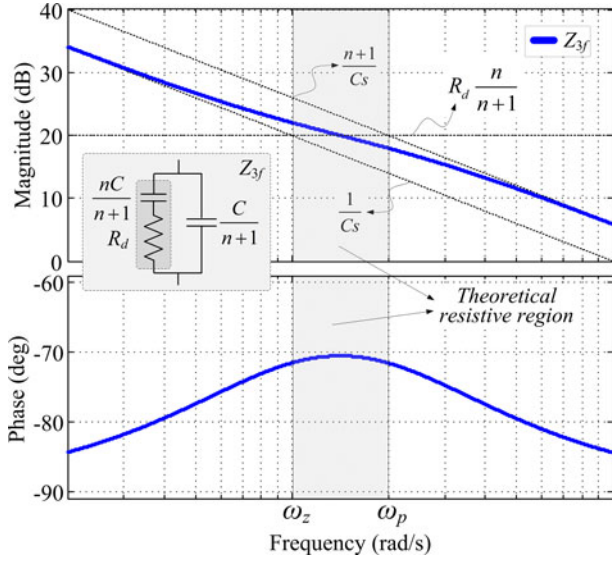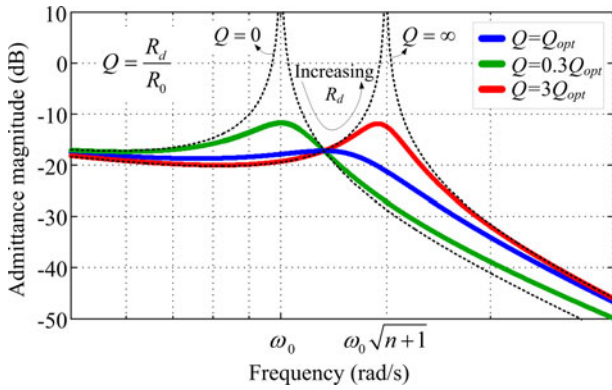
Fig. 4. Generalized phase and magnitude of the parallel impedance Z_{f3}.

Fig. 5. Generalized forward transadmittance magnitude of the *LCL* filter with shunt *RC* damper.

frequencies that define the resistive region of the damper can be derived as [23]

$$\omega_z = \frac{n+1}{nR_dC} \tag{11}$$

$$\omega_p = \frac{(n+1)^2}{nR_dC}. \tag{12}$$

In Fig. 5, the filter forward transadmittance of the overall filter is shown with varying the damping resistor. Therefore, a typical characteristic of a filter which uses multisplit capacitors or inductors in addition to the damping resistor is the different peaks that are exhibited by the filter depending on the value of the damping resistor. For instance, increasing the resistor value from zero to infinite will not only increase the frequency of the filter resonance and decrease the high-frequency attenuation, but also the filter may exhibits one of the two characteristic frequencies described in the following. When the resistor is close to zero, the resonance amplitude and frequency is about

the same as the characteristic frequency of the filter. However, when the resistor increases and its values becomes very large the resonance amplitude approach again infinity but at a different frequency given mainly by the filter capacitor $C_f = C/(n+1)$.

1) Optimum Frequency: The filter characteristic exhibits a minimum in the forward transadmittance at a specific frequency, when the quality factor is optimally selected. In the following, the specific frequency is called optimum since at this frequency the minimum peak in the filter admittance occurs. From Fig. 5, it can be seen that the minimum peak exists at a frequency given by the intersection of the filter admittance characteristics when the resistor is zero and infinite, respectively, both defined as

$$Y_{21}\big|_{R_d=0} = Y_0 \frac{1}{\frac{s^2}{\omega_0^2}+1} \tag{13}$$

$$Y_{21}\big|_{R_d=\infty} = Y_0 \frac{1}{\frac{s^2}{(n+1)\omega_0^2}+1}. \tag{14}$$

Making equal the two transfer functions given in (13) and (14), the optimum frequency can be computed as

$$\left|\frac{s^2}{\omega_0^2}+1\right|_{s=j\omega_{\mathrm{opt}}} = \left|\frac{s^2}{(n+1)\omega_0^2}+1\right|_{s=j\omega_{\mathrm{opt}}}$$

$$\rightarrow \omega_{\mathrm{opt}} = \omega_0\sqrt{\frac{2(n+1)}{n+2}}. \tag{15}$$

From (15), it can be seen that with properly designed *RC* damper the actual resonance frequency of the filter ω_{opt} can be easily determined mainly as function of the ratio between the damping and filter capacitor, defined as

$$n = \frac{C_d}{C_f}. \tag{16}$$

2) Peak in the Filter Admittance: The magnitude of the peak in the filter admittance can be obtained by replacing the Laplace operator in (13) with the optimal frequency from (15)

$$|Y_{21}|_{\omega=\omega_{\mathrm{opt}}} = \frac{1}{\omega_0(L_1+L_2)}\sqrt{\frac{(n+2)^3}{2(n+1)n^2}}. \tag{17}$$

In case the peak in the filter admittance is not minimum, then the damping is called suboptimal and (17) is not valid.

3) Optimal Quality Factor: With the optimal frequency known, the question in hand is how to derive the quality factor to achieve the minimum peak in the filter forward transadmittance. The derivative of the filter admittance magnitude from (9) with respect to the optimum frequency of the filter will result in the optimal quality factor as indicated by

$$\left[\frac{d}{d(x^2)}|Y_{21}|^2\right]_{\begin{cases} s=j\omega_{\mathrm{opt}} \\ x=\frac{\omega_{\mathrm{opt}}}{\omega_0}=\sqrt{\frac{2(n+1)}{n+2}} \end{cases}} = 0 \tag{18}$$

$$Q_{\mathrm{opt}} = \sqrt{\frac{(5n+4)(n+2)(n+1)}{2n^2(-n+4)}} \quad \text{for } n \in (0, 1.3]. \tag{19}$$
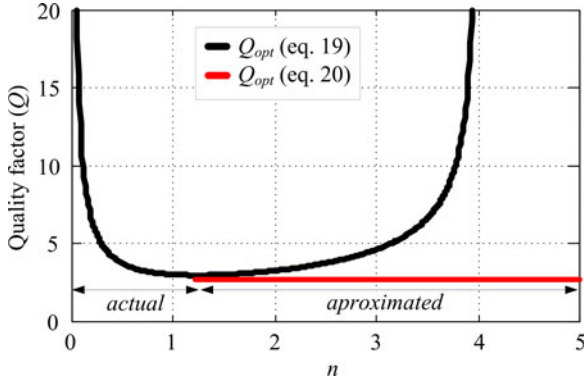
Fig. 6.   Optimal quality factor of the *LCL* filter with *RC* damper shunt.

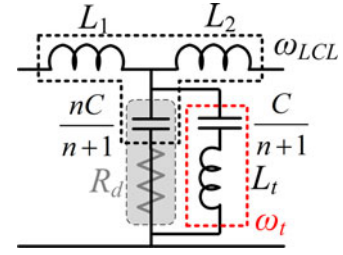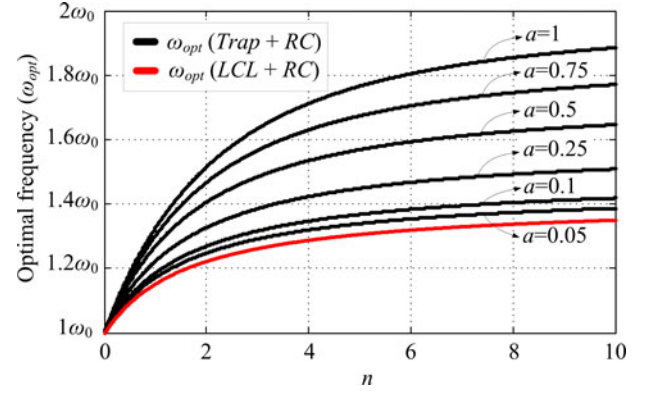Fig. 7.   Per phase schematics of the trap filter with *RC* damper when $Q = 0$.

Fig. 8.   Map of the optimal frequency for the *trap* filter with *RC* damper shunt and comparison with the *LCL* filter.

However, proceeding with the derivation of the filter admittance, the following result occurs. For *n* higher than 1.3 no peak occurs in the filter admittance; hence, the derivations are not valid after $n = 1.3$. The derivations developed by Middlebrook for the *LC* filter holds for any value of *n* due to the fact that the transfer functions of the *LC* filters always exhibits a peak, whatever the ratings of the filter. In the case of higher order filters such as the *LCL* filter, adopting optimum damping for $n > 1.3$ will eliminate the peaks from the filter admittance. As result, the transfer function will continuously decrease over the entire frequency range of interest. Thankfully, for $n > 1.3$ the quality factor can be approximated as

$$Q_{\mathrm{opt}} \simeq 2.5 \ \text{for} \ n \in [1.3, \infty). \tag{20}$$

The motivation is in the fact that with increasing *n*, the damping and therefore the quality factor is less influenced by the value of the damping resistor. Additionally, large values of *n* are not typical used in practice, since higher losses will occur in the resistor due to a more significant current in the damping capacitor then the filter capacitor. The variation of the optimal quality factor as function of the filter capacitors ratio is illustrated in Fig. 6.

C. Shunt RC Damper for Trap Filters

The same procedure can be applied for the *trap* filter. The main difference in this case lie in the fact that the optimal frequency and optimal quality factor has a 2-D dependence on the capacitors ratio of the filter and on the ratio between the trap inductance L_t and the equivalent inductance of the filter *L*, defined as

$$a = \frac{L_t}{L}. \tag{21}$$

By making equal the filter admittance when the resistor is zero and infinite, respectively, the optimal frequency results as indicated in (25), shown at the bottom of the next page.

However, when the resistor is zero, the filter admittance exhibits two peaks at two frequencies given by

$$\omega_{0(1)} = \sqrt{\frac{A + B - \sqrt{(A - B)^2 + \frac{4AB}{n+1}}}{2n}} \tag{22}$$

$$\omega_{0(2)} = \sqrt{\frac{A + B + \sqrt{(A - B)^2 + \frac{4AB}{n+1}}}{2n}} \tag{23}$$

where

$$\begin{cases} A = \omega_{0(LCL)}^2 n = (n + 1) \dfrac{L_1 + L_2}{L_1 L_2 C} \\[2mm] B = (n + 1) \omega_t^2 = \dfrac{(n + 1)^2}{L_t C}. \end{cases} \tag{24}$$

Therefore, in (25), the intersection around the first peak in the filter admittance is considered for the optimal frequency derivation. The equivalent circuit of the filter with the resistor bypassed is illustrated in Fig. 7.

A map of the optimal frequency of the *trap* filter as function of the capacitors ratio, the inductance ratio, and the optimal frequency of the *LCL* filter defined in (15) is illustrated in Fig. 8. It should be noted that the characteristic frequency (ω_0) correspond to the values given in Table I and not to the frequencies defined in (22)–(23). The derivation of the optimal quality factor leads to a rather lengthy equation and is omitted here for simplicity. However, a map of the optimal quality factor is illustrated in Fig. 9 which can be easily used for any ratings of the passive filter,

It can be seen that the quality factor is lower than the *LCL* filter quality factor and the decrease depends mainly on the trap inductance value. If $L_t << L$, then both the optimal frequency and the quality factor can be approximated with the *LCL* filter
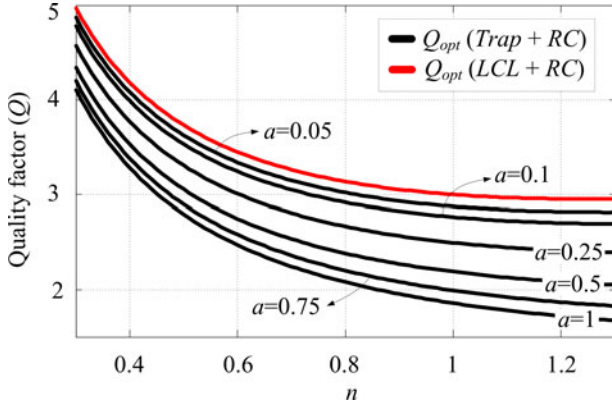
Fig. 9. Map of the quality factor for the *trap* filter with *RC* damper shunt and comparison with the *LCL* filter.
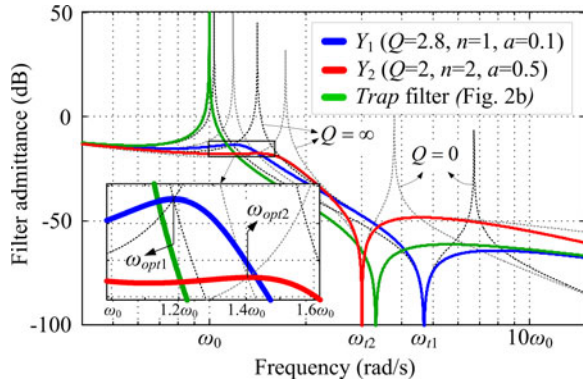

Fig. 10. Examples of *trap* filter admittances for two different designs: $n = 1$ and $a = 0.1$ and $n = 2$ and $a = 0.5$.

optimal frequency and the quality factor defined in (15) and (19)–(20), respectively.

An example on how to use the optimal frequency and optimal quality factor maps is explained in the following. Let us assume a damping circuit with the ratios of the filter capacitors and inductors given as $n = 1$ and $a = 0.1$. From Fig. 9, the quality factor is around 2.8 while the frequency from Fig. 8 is around 1.2 ω_0. Another example can be $n = 2$ and $a = 0.5$. In this case, the quality factor is out of the map range defined in Fig. 9. However, since with larger n, the optimal quality factor can be considered constant from Fig. 9, the quality factor can be extrapolated to around 2 while the frequency from Fig. 8 results around 1.4 ω_0. Then, the damping resistor value can be computed from the quality factor, i.e., $R_d = R_0 Q$. The two examples of the resulted filter admittances are illustrated in Fig. 10.

Since the inductors ratio a is different for the two considered examples, the trap frequencies also results different. When the quality factor is zero, it can be noticed the two peaks in the

filter defined by (22)–(23). However, with the use of the shunt *RC* damper, their amplitude becomes low and there is no risk of amplification of other harmonics that are present in the converter voltage. Additionally, in Fig. 10, the undamped *trap* filter admittance from Fig. 2(b) is illustrated. In order to simplify the derivations, the optimal frequency of the *trap* filter with shunt *RC* damper is referred to the characteristic frequency (ω_0) of the undamped *trap* filter in (22).

D. Limitations

By considering the suboptimal damping case of the *LCL* filter with shunt *RC* damper from Fig. 5 when $Q = 0.3Q_{\mathrm{opt}}$ and $Q = 3Q_{\mathrm{opt}}$, one could assume that the resonance frequency and magnitude of the filter admittance is optimum. Then, the damping circuit ratings (n, C, R_d) can be refined to obtain the minimum peak as follows. The magnitude of the filter at the optimum frequency can be written from (17) as a function of the new characteristic frequency of the filter ω_{0_new}

$$|Y_{21}|_{\omega=\omega_{\mathrm{opt}}} = \frac{1}{\omega_{0\_\mathrm{new}}(L_1+L_2)} \sqrt{\frac{(n+2)^3}{2(n+1)n^2}}. \quad (26)$$

The value of the new characteristic frequency of the filter can be derived from (15), in which the optimum frequency is the resonance frequency of the suboptimal damping case $Q = 0.3Q_{\mathrm{opt}}$ and/or $Q = 3Q_{\mathrm{opt}}$

$$\omega_{0\_\mathrm{new}} = \omega_{\mathrm{opt}} \sqrt{\frac{n+2}{2(n+1)}}. \quad (27)$$

By substitution of (27) into (26), the new ratio between the capacitors (n_{new}) results as

$$n_{\mathrm{new}} = \frac{2}{|Y_{21}|_{\omega=\omega_{\mathrm{opt}}} \omega_{\mathrm{opt}}(L_1+L_2)-1}. \quad (28)$$

By writing the characteristic frequency from (27) as function of the filter components, the value of the refined capacitor value can be taken from the characteristic frequency of the filter ω_{0_new} as

$$C_{\mathrm{new}} = \frac{2(n_{\mathrm{new}}+1)(L_1+L_2)}{(n_{\mathrm{new}}+2)L_1 L_2 \omega_{\mathrm{opt}}^2}. \quad (29)$$

From Fig. 5, one can substitute the magnitude of the filter admittance and its corresponding frequency for the two suboptimal cases in (28) to find the new ratio between the two capacitors. Then, with (29), the refined value of the total filter capacitance can be found. The value of the damping resistor can be found from the quality factor of the filter given in (19). In Fig. 11, the refined filter transfer functions with the optimum parameters are plotted against the two suboptimal cases when $Q = 0.3Q_{\mathrm{opt}}$ and $Q = 3Q_{\mathrm{opt}}$. A summary of the main features

$$\omega_{\mathrm{opt}} = \omega_0 \sqrt{-(n+1)(a+1)\frac{-2a-n-2+\sqrt{4a(a-n+2)+(n+2)^2}}{2an}} \quad (25)$$
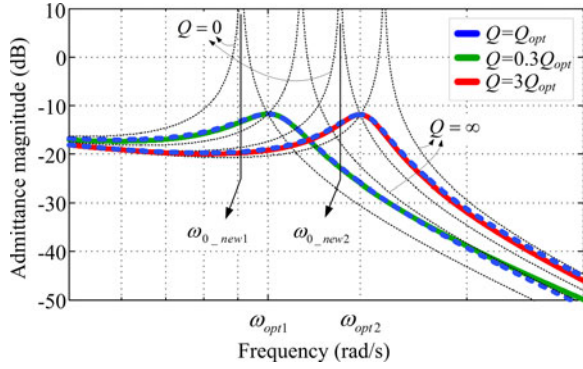
Fig. 11. Optimal versus suboptimal design of the damping circuit for the *LCL* with *RC* damping shunt.

TABLE II
DAMPING CIRCUIT RATINGS IN THE CASE OF OPTIMAL
AND SUBOPTIMAL DAMPING

Type of damping	C(PU)	Damping Losses (PU)	$W_{pk(Rd)}$ (PU)	Switching harmonics (PU)	n
Suboptimal damping 1: $Q = 0.3Q_{opt}$	1	0.52	0.85	0.79	1
Optimal damping 1	1.2	0.69	0.57	0.61	0.51
Suboptimal damping 2: $Q = 3Q_{opt}$	1	2.58	1.44	1.03	1
Optimal damping 2	0.6	0.27	0.38	1.16	0.35

for the two optimal and suboptimal damping scenarios is given in Table II, with the ratings of the damping circuits given in Per Unit (PU) and referred to the optimal case from Fig. 5. The main objective is to illustrate different feature trends in adopting several optimal damping solutions. If minimum peak in the filter admittance is selected in the design, then a lower damping capacitor C_d and a lower rated damping resistor is obtained compared to the suboptimal case, fact which is also verified in dc–dc applications [21]. If a suboptimal damping is chosen, i.e., $Q = 3Q_{opt}$, then the damping losses will increase 2.5 times and the watt-peak of the resistor $W_{pk(Rd)}$ increases with 50%.

On the other hand, a corresponding optimum solution will lead to a reduction of the damping losses to about four times and of the resistor ratings to about three times. A disadvantage of the optimal solution will be in the amplification of the switching harmonics, if an *LCL* filter is adopted. For the *trap* topology, since infinite attenuation is theoretically possible, the influence on the high-frequency harmonics will be less significant. If the quality factor is chosen lower than the optimal, e.g., $Q = 0.3Q_{opt}$ the differences between the optimal and suboptimal solutions are more balanced. From the design point of view, adopting the proposed design method will lead to less iterations to find the damping parameters, since all the information can be taken from the capacitors ratio and/or trap inductance ratio. In addition, the actual resonance frequency of the filter is known, which provides more insight compared to the characteristic frequency of the filter. Furthermore, the design is generalized for any ratings of the filter or grid impedance (the equivalent inductance of the grid impedance is considered in the filter grid
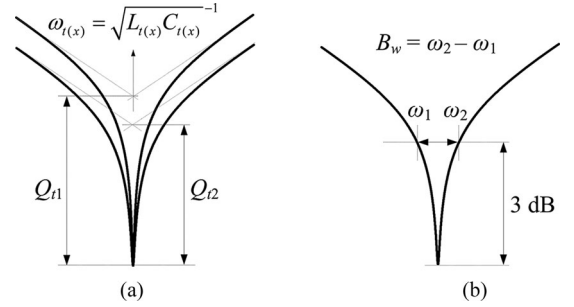

Fig. 12. Characteristic impedance of series tuned traps: (a) provided same inductance/resistance and $Q_{t1} = 50$, $Q_{t2} = 25$; (b) definition of the bandwidth parameter.

side inductor). Similar derivations can be obtained for input admittance of the filter.

IV. IMPROVED DESIGN METHOD OF THE MULTITUNED *Traps* FILTER

A. Conventional Design of the Individual Traps Based on the Trap Quality Factor

One criteria to design the individual traps in a multituned *trap* filter is the quality factor of the individual traps [25], which should be in the range of $10 \leq Q_{t(x)} \leq 50$ [9], [25], where $Q_{t(x)}$ denotes the quality factor of the *x*-tuned trap defined as

$$Q_{t(x)} = \frac{1}{R_{t(x)}} \sqrt{\frac{L_{t(x)}}{C_{t(x)}}} \qquad (30)$$

where $L_{t(x)}$ is the tuned inductor, $C_{t(x)}$ the tuned capacitor, and $R_{t(x)}$ the equivalent resistor of the tuned trap, mainly given by the *ESR* of the inductor and wiring resistance in the tuned trap. Therefore, assuming a fixed inductance, the quality factor varies only with the tuned capacitance. The characteristic impedance of a tuned trap is illustrated in Fig. 12(a) for two different capacitances together with the definition of the bandwidth parameter B_w which describes how broad is the filtering action [see Fig. 12(b)]. Therefore, with the bandwidth and quality factor information it becomes apparently easy to design the tuned traps. However, both the bandwidth and quality factor imply complete knowledge of the trap resistance which is more difficult to be accurately calculated. Furthermore, values of the quality factor as recommended in [9] and [25] typically applies for series tuned traps used to compensate individual low-order harmonics that are presented in the grid. For a grid-connected VSC, the tuned trap is responsible to reduce the entire spectrum of dominant sideband harmonics around the switching frequency or multiples. An example of trap admittance characteristic used in grid-connected applications and which is tuned around the switching frequency of the VSC is shown in Fig. 13 with varying the trap resistance.

From Fig. 13, it can be identified that the choice of trap resistance value (and therefore the quality factor) does not significantly influences the attenuation of dominant harmonics. Therefore, a design procedure with the quality factor/bandwidth in mind could turn tedious, especially if more than one trap is
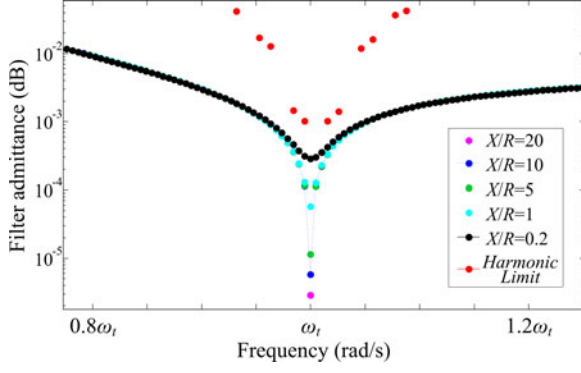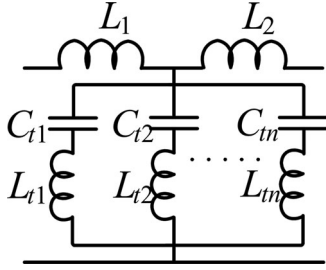
Fig. 13. Filter admittance around the tuned frequency of the first trap.

Fig. 14. Per phase schematics of a multituned *trap* filter.

used. The harmonic limit in Fig. 13 is the admittance of the filter required to meet IEEE 1547 harmonic specifications [26], i.e., admittance given by the harmonic current limit given in [26] divided to the harmonic spectrum of the converter voltage computed for the sidebands harmonics as $m_f \pm 2, m_f \pm 4, m_f \pm 8$, etc.

B. Improved Design Method Based on Individual Functions of the Multisplit Capacitors

It was shown in Fig. 12 how with increasing capacitance of a tuned trap, the bandwidth of the filter increases, i.e., a broader attenuation is obtained from the filter. This fact is used to design the multituned traps, by adequately splitting the filter capacitors such that the switching harmonics are effectively reduced. In Fig. 14, a multituned *trap* filter is illustrated. The design problem of the multisplit capacitors for an *n*-trap filter is given by
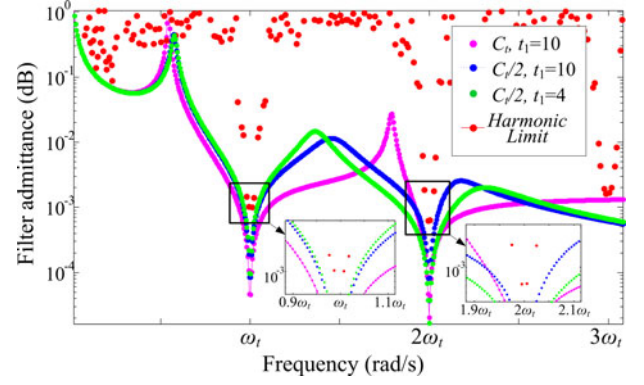
$$\sum_{x=1}^{n} C_{t(x)} = C_t \tag{31a}$$

$$C_{t1} = t_x C_{t(x+1)}\big|_{x=1..n-1} \tag{31b}$$

$$t_x \geq \left(\frac{\omega_{t(x+1)}}{\omega_{t1}}\right)^2\bigg|_{x=1..n-1} \tag{31c}$$

$$C_{t1} = \frac{C_t}{1+\sum_{x=1}^{n-1}\frac{1}{t_x}} \tag{31d}$$

$$C_{t(x+1)} = \frac{C_t}{1+\sum_{x=1}^{n-1}\frac{1}{t_x}}\frac{1}{t_x}\bigg|_{x=1..n-1}. \tag{31e}$$

In (31a), the sum of the individual trap capacitances equals to the total capacitance of the traps C_t; the split factor t_x is introduced in (31b) and defines how many times the capacitance in

Fig. 15. Examples of a *two trap* filter admittances for different trap capacitances (C_t) and split factors (t_1).

the trap tuned around the switching frequency is larger than the capacitance of $(x + 1)$—trap tuned around the multiple of the switching frequency; the previous precondition leads to the conservative limit of the split factor given in (31c) which ensures that the bandwidth of the $(x + 1)$—trap does not exceed the bandwidth of the first trap; the value of the individual *x*—trap capacitance as function of the total capacitance of the traps is given in (31d) and (31e). For a two *trap* filter with the individual traps tuned around the switching and twice the switching frequency, the design problem defined in (31) reduces mainly to

$$C_{t1} + C_{t2} = C_t \tag{32a}$$

$$C_{t1} = t_1 C_{t2} \tag{32b}$$

$$t_1 \geq \left(\frac{\omega_{t2}}{\omega_{t1}}\right)^2 \simeq 4 \tag{32c}$$

$$C_{t1} = \frac{C_t}{1+\frac{1}{t_1}} = \frac{t_1}{t_1+1}C_t \tag{32d}$$

$$C_{t2} = \frac{C_t}{1+\frac{1}{t_1}}\frac{1}{t_1} = \frac{1}{t_1+1}C_t. \tag{32e}$$

Therefore, for a two *trap* filter, the critical design parameter reduces to finding the split factor t_1 that ensures effective reduction of the switching harmonics. The split factor choice is critical due to the fact that it specifies how the two individual traps suppress the switching harmonics. In [10] and [25], relatively close values of the trap capacitors have been suggested for the multituned *trap* filter ($1 \leq t_1 \leq 2$). Another solution is to adopt the conservative limit, i.e., $t_1 = 4$ as also was used for the *LTCL* filter in [25], which ensures same bandwidth for the two traps. However, both solutions will not result in the most desirable solution since the second trap will have a broader attenuation compared with the first trap. This is equivalent to a larger capacitance than actually needed, which finally results also in larger inductor since with higher capacitance, the current increases in the second trap. In this design method, it is suggested a split factor that ensures similar attenuation of the switching harmonics in the tuned traps, i.e., the tuned traps must have about the same broader attenuation around the most dominant harmonics. In Fig. 15 is shown an example of a two *trap* filter admittance for the conservative limit of the split factor and the proposed split factor with varying the total capacitance.

It can be seen that once the split factor is properly designed, changing the total trap capacitance influences in the same way the attenuation of individual traps, so adjustments of the split factor are not necessary with changing the filter capacitance.

For a given total capacitance of the filter, the split factor can be computed from the harmonic limit requirement while the total capacitance can be adjusted afterward based on the required attenuation of the filter, susceptibility of the filter toward the tolerances in the passive components, variation of the grid impedance, etc.

C. Resonance Damping for Multituned Traps Filter

To damp the resonances in a multituned *trap* filter, the *RC* damper shunt is adopted. Then, the equivalent circuit of the filter is the same as presented in Fig. 2(f). Since the filter transfer function of a multituned *trap* filter is of very high order (sixth order for a two *trap* filter), the characteristic frequency of the filter is simplified to

$$\omega_0 \simeq \sqrt{\frac{1}{(C_d + C_{t1})\left(\frac{L_1 L_2}{L_1 + L_2} + L_{t1}\right)}}. \qquad (33)$$

The previous approximation ignores the influence of the traps tuned around the multiples of the switching frequency since their influence affects mainly the high frequency of the filter (well above the resonance frequency of the filter). Then, the optimum frequency map from Fig. 8 can be used to find the optimum frequency of the filter. Similarly, the quality factor map given in Fig. 9 can be used to find the quality factor of the filter, provided that

$$a = \frac{L_1 + L_2}{L_1 L_2 \sum_{x=1}^{n} \frac{1}{L_{t(x)}}}. \qquad (34)$$

The damping resistor value results from the quality factor as

$$R_d = Q_{\text{opt}} \sqrt{\frac{1}{C}\left(\frac{L_1 L_2}{L_1 + L_2} + \left(\sum_{x=1}^{n} \frac{1}{L_{t(x)}}\right)^{-1}\right)}. \qquad (35)$$

V. DESIGN EXAMPLE OF THE PASSIVE DAMPED *LCL*, *Trap*, AND *Multituned Trap* FILTER

An overall design procedure of a high-order filter in the presence of a passive damping circuit is covered in the following. First, a two-level 10-kW VSC, with 10-kHz switching frequency, 700-V dc-link voltage, 400-V line-to-line grid voltage and conventional space vector modulation (SVM) is adopted. In this design, the filter design is done independently of the converter. Therefore, the ratings of the converter are used as input parameters for the filter design. For this power level, it is expected a total power loss in the range of around 1% in the passive filter, according to [27]. The attenuation of the high-frequency switching components is done according to the harmonic limits defined in IEEE Std. 1547–2008 [26] (up to 0.3% permissible current for harmonics order higher than 35, for a short-circuit

ratio of 20). For attenuation of the resonance frequency components, a low-quality factor of the filter ($Q \approx 2 - 5$) is needed to limit the peaks in the filter admittances and to ensure a good control performance. Typically, the peaks should be limited to around –5 and –10 dB [28].

A. Design of the Main Filter

In the following, the percentage of the base values are used for the filter components calculation as presented in [1].

1) Converter Side Inductance: The design of the converter side inductance is limited to the current ripple requirement in the inductor which depend mainly on the switch current and size of the filter which reduces with increasing the ripple. For the SVM, the maximum current ripple occurs when the voltage reference vector is aligned with the switching vector; therefore, when the reference angle is zero. Taking into account, the available dc-link voltage, the switching frequency, and the modulation index ($M \approx 0.9$) the current ripple can be written based on the volt-second balance across the inductor as

$$\Delta I_1 = \frac{V_{\text{DC}}}{4 L_1 f_{\text{sw}}}\left(\frac{2}{3}M - \frac{M^2}{2}\right)\sin\left(\frac{\pi}{3}\right) \simeq \frac{V_{\text{DC}}}{24 L_1 f_{\text{sw}}} \qquad (36)$$

which assume low-voltage drop across the grid side inductance (voltage across the capacitor in phase with the grid voltage). The inductance results in the range of 3% by adopting a 10% current ripple. The peak current rating of the inductor which should avoid the saturation of the magnetic core results as

$$I_{L1(pk)} \simeq \sqrt{2}I_{\text{rated}} + \Delta I_1 = \frac{A_c B_{\text{max}} N}{L_1} \qquad (37)$$

where the maximum operating flux density of the inductor is lower than the saturation flux density of the core ($B_{\text{max}} < B_{\text{sat}}$); A_c is the cross-sectional area of the core, N number of turns, and I_{rated} the rated current of the VSC.

2) Filter capacitance value: The capacitor value for 5–10-kHz switching frequency applications is typically limited to 5% in order not to decrease the power factor and demand high fundamental current from the filter because of a too large capacitance [1]. Considering the standardized ratings of capacitors, a 4.7% capacitor is adopted. The same capacitance is adopted for the *trap* and multituned *trap* filter. For the multituned *trap* filter, a split factor t_1 of 10 is adopted based on the considerations from the previous section. Since passive damping is adopted, it is not required to compute the trap inductances at this stage since the capacitance has to be split once more time because of the damping capacitor.

3) Line Inductance Value: The line inductance is computed considering the attenuation of the filter. For example, if the grid current around the switching frequency is limited to 0.3%, then L_2 can be computed from (4) considering the voltage spectrum $V_1(h)$ corresponding to the SVM at the most dominant harmonic order ($m_f - 2$) as

$$L_2 \geq \frac{2\pi f_1 h L_1 \frac{0.003 I_{\text{rated}}}{V_1(h)} + 1}{2\pi f_1 h \left(L_1 C (2\pi f_1 h)^2 - 1\right)\frac{0.003 I_{\text{rated}}}{V_1(h)}}\Bigg|_{h = m_f - 2} \qquad (38)$$

where m_f is the modulation frequency index and f_1 is fundamental frequency. Considering that for SVM, $V_1\,(m_f - 2) \approx 18.5\%$ under rated conditions, then from (38) a minimum value of the grid side inductance which ensure the harmonic requirement is 0.7%. Since the presence of passive damping decrease the high-frequency attenuation of the filter, a 1.4% is adopted in the first step. Similarly, the line inductance for the *trap* and multituned *trap* filter can be calculated. Otherwise, a good starting point is to consider a half-line inductance for the *trap* filter and a quarter for the multituned *trap* filter, from the *LCL* line inductance. Finally, the total percentage inductance should not exceed the total percentage capacitance in order to limit the volume of the overall filter [29]

$$L_{1(\%)} + L_{2(\%)} \le C_{\%}. \tag{39}$$

B. Design of the Damping Circuit

The damping design problem reduces to the proper choice of the ratio of the damping capacitor to the filter capacitor as defined in (16). For a given ratio of the capacitors n, the *trap* filter capacitance can be found using

$$C_t = \frac{1}{n+1}C. \tag{40}$$

Then, the individual trap capacitances of the multituned *trap* filter can be found using the split factor function defined in (32d) and (32e). The corresponding tuned inductances can be derived from

$$L_{t(x)} = \frac{1}{C_{t(x)}\omega_{t(x)}}. \tag{41}$$

With the trap inductances, the ratio of the trap inductance to the filter inductance a can be found from (21) and (34). The optimal quality factor and the optimal frequency of the filters can be found from Figs. 8 and 9. Finally, the value of the damping resistor can be found from the quality factor as

$$R_d = R_0 Q_{\text{opt}}. \tag{42}$$

Since all the damping parameters depend at this point on the capacitors ratio n, it is important to choose a ratio which ensure an optimal choice of the damping circuit ratings, i.e., ratings which are not impairing the features of the filter. For a damping circuit, the critical features are related to the degradation of the high-frequency attenuation of the filter, losses in the damping circuit, and the peak of the filter admittance.

1) Degradation of the Filter High-Frequency Attenuation: In Fig. 16, the attenuation of the most relevant dominant switching harmonics is illustrated for the proposed filter topologies with changing the ratio of the capacitors. To match the harmonic attenuation of the *LCL* filter, in case of the *trap* filter the line inductance is reduced to 0.6% while for the *two traps* the filter inductance is reduced to 0.4% in addition to the converter side inductance which is reduced to 1.5%. The limit factor in case of the *trap* filter is the attenuation around the $(x + 1)$ multiple of the switching frequency, where x is the highest order of the tuned trap used in the filter.
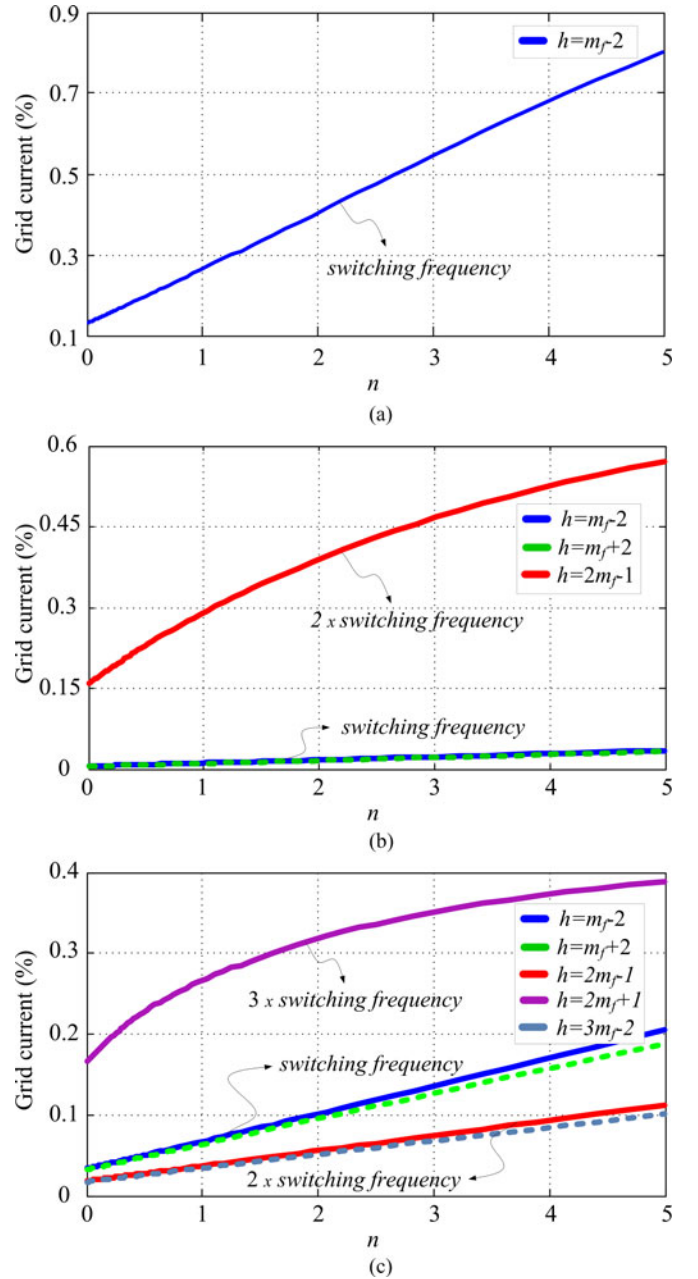

Fig. 16. Grid current harmonics as function of the capacitor ratio: (a) *LCL* with *RC* damper shunt, (b) *Trap* with *RC* damper shunt, (c) *Two traps* with *RC* damper shunt.

2) Damping Losses: The damping losses in the damping circuit are calculated analytically following the principle given in [19]. In Fig. 17, the damping losses are illustrated for the proposed filters with varying the capacitors ratio. With increasing the number of tuned traps, the passive damping losses decreases as lower harmonic current flows in the resistor branch. It is expected the higher damping losses with increasing n, since the damping capacitor is also proportionally increased.

3) Peak in the Filter Admittance: The optimum frequency can be used to derive simple formulations for the filter admittance magnitude at the resonant frequency, as given in (17).
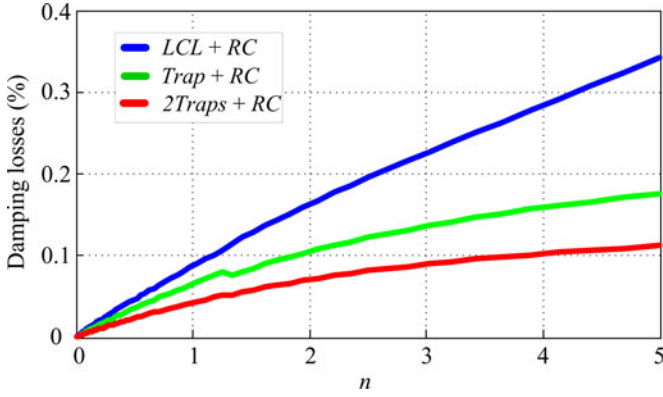
Fig. 17. Damping losses as a function of the capacitor ratio for the three topologies calculated according to [19].
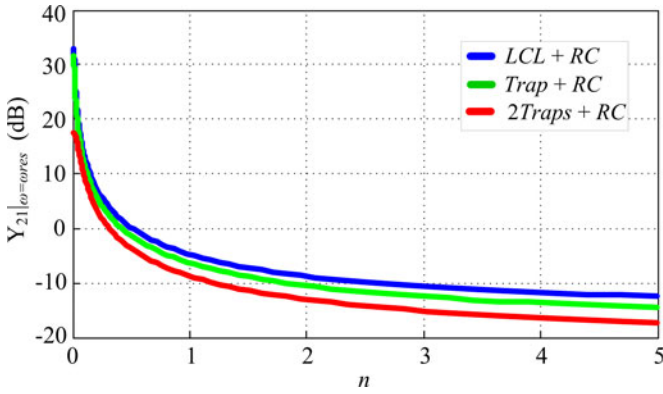

Fig. 18. Open loop transfer function magnitude of the resonance peak as a function of the capacitor ratio for the three topologies.

Fig. 19. Root loci of the closed-loop current control under ideal conditions and worst-case scenario for the *trap* filter with shunt *RC* damper.

TABLE III
FILTER RATINGS BASED ON THE PROPOSED DESIGNED METHOD (PER PHASE)

Filter	Passive Device	Peak Rating	L/C/R	LI^2 (HA^2)	Volume (cm^3)
LCL + RC	L_1	23 A	1.5 mH	1.06	513
	L_2	21 A	0.7 mH		200
	C_d, C_t	330 V	4.7 μF		22.7
	R_d	17 W	17 ω		–
Trap + RC	L_1	23 A	1.5 mH	0.89	513
	L_2	21 A	0.3 mH		100
	C_d, C_t	330 V	4.7 μF		22.7
	L_t	3 A	0.05 mH		7.6
	R_d	14 W	13 ω		–
2Traps + RC	L_1	25 A	0.8 mH	0.59	200
	L_2	21 A	0.2 mH		100
	C_d, C_t	330 V	4.7 μF		22.7
	L_t	5 A	0.05 mH		7.6
	C_{t2}	330 V	0.44		3.65
	L_{t2}	2.5 A	0.14 mH		7.6
	R_d	17 W	7.7 ω		–

Below the Nyquist frequency, the peak in the filter admittance can be analyzed considering the open loop current controller as indicated in (2) in order to identify the influence of the passive damping design in the controller stability. Therefore, in Fig. 18, the open loop magnitude is illustrated, provided that the current controller is tuned with technical optimum criterion [30] ($K_p \approx f_s(L_1 + L_2)/3$) and the delay it is assumed as 1.5 sampling periods.

4) Discussion on the Choice of the Filter Capacitors Ratio: From Fig. 18, it can be seen that with increasing the capacitors ratio, also the peak reduces in the filter admittance. A value of n between 0.4 and 1.5 seems a reasonable choice since outside this range either the admittance peak exponentially increases (low n) or is relatively constant (with large n). The same range can be used also for the damping losses and filter attenuation since the losses are lower than 0.1% and the harmonic limit are close to imposed limit of 0.3%. However, the critical choice is to find out if the choice of the capacitors ratio ensures the current control stability for a given operating conditions. An initial guess is an equal ratio between the filter capacitors ($n = 1$).
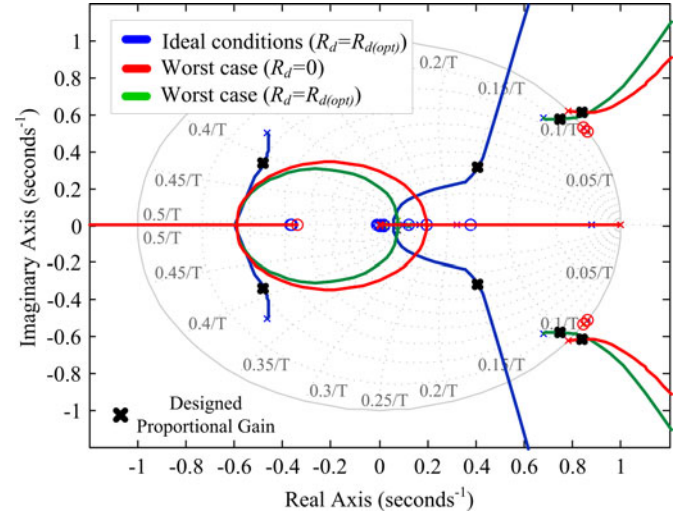
C. Verification of the System Stability Under Actual Operating Conditions

To test the system stability under actual operating condition, it is considered in the following that:
1) the grid equivalent inductance varies in the range of 0.6–5% (calculated from the base inductance of the VSC);
2) the permeability decrease of the filter inductors is 30% (in low load condition the inductance is 130%);
3) the tolerances of the passive components are $\pm$30% for the inductors and $\pm$20% for the filter capacitors.

A worst-case scenario can be low load condition, high-grid impedance condition, and increased tolerances in the passive components. This translates to a value of 170% of the designed filter inductors, 120% of the filter capacitance in addition to the grid inductance which for the *trap* filter is 4.4% (the minimum value of the grid inductance is considered part of the filter inductance L_2). As illustrated in Fig. 19, the root loci of
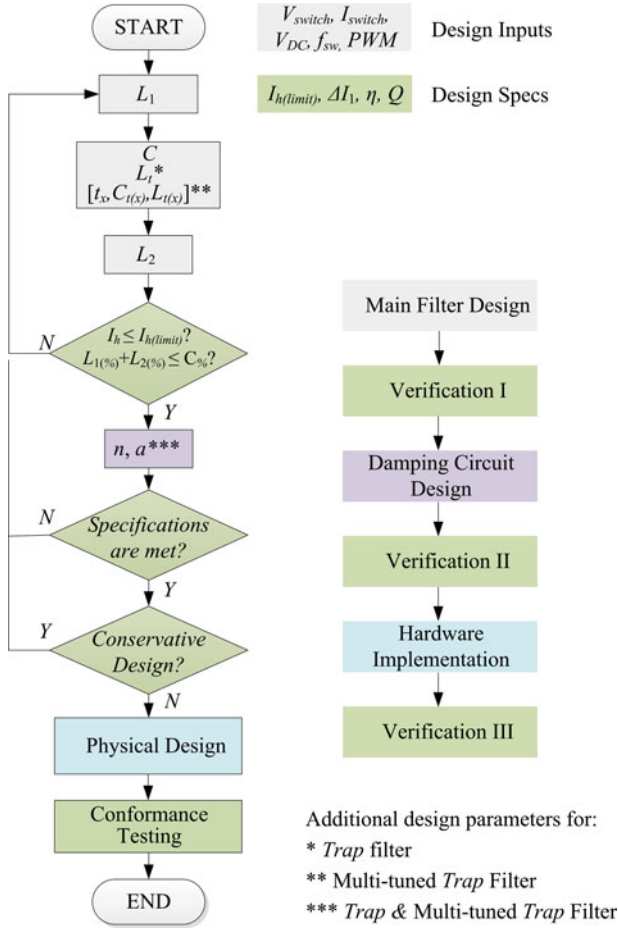
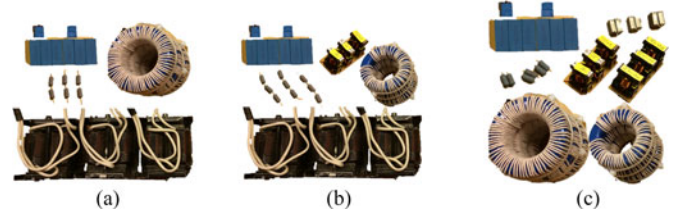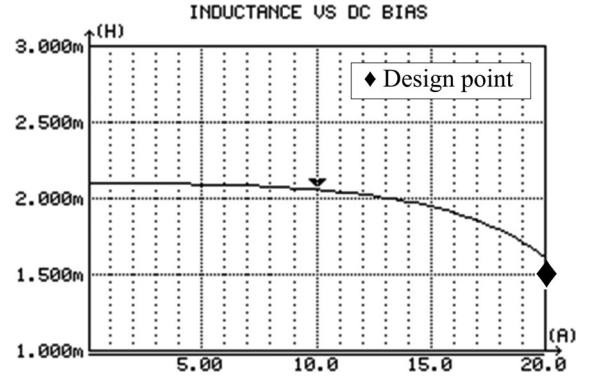Fig. 20. Flowchart of the proposed design method for high-order filters.

TABLE IV
MEASURED POWER LOSS AND POWER QUALITY INDICES (%)

Description	$LCL + RC$	$Trap + RC$	$2Traps + RC$
Total Losses	1	1	0.95
Damping Losses	0.075	0.071	0.053
THD_{v2}	0.45	0.45	0.39
THD_{i2}	1.27	1.12	2.67
$I_{2(mf-2)}$	0.083	0.0083	0.0328

Fig. 21. Passive filters prototypes: (a) *LCL* with shunt *RC* damper, (b) *Trap* with shunt *RC* damper, (c) *Two traps* with shunt *RC* damper.

Fig. 22. DC-bias test of the *LCL* and *trap* filters converter side inductance.

the closed-loop current control under ideal conditions, under the worst-case scenario ($L_1 = 5.1\%$, $L_2 = 5\%$, $C = 5\%$), and under worst-case scenario with no passive damping ($R_d = 0$). Under ideal conditions, the current controller has a damping factor of 0.707 according to the technical optimum design criterion. However, with increasing the ratings of the passive components toward the worst-case parameters drift, the controller approach to instability boundary while with disconnecting the damping resistor, the current controller become unstable. Similar, results are obtained for the other two filter topologies or by adopting decreased tolerances in the passive components. Therefore, it can be concluded that the initial choice of $n = 1$ is correct, since the system is stable under the worst-case scenario.

D. Summary of the Proposed Filter Design

The final solution chosen in this design is $n = 1$ for the *LCL* and *trap* filters with shunt *RC* damper and $n = 1.094$ for the *two traps* topology, according to the standardized ratings of the capacitors. The final choice of n ensures that the switching harmonics are limited just below the 0.3% limit, while the peak in the open loop transfer function is well limited below –5 dB. The final ratings of the passive components after the physical design of the inductors are shown in Table III. A generalized

flowchart of the proposed filter design method with the optimal passive damping is illustrated in Fig. 20.

VI. EXPERIMENTAL RESULTS

A. Setup Description

To demonstrate the filter design, a 10-kW Danfoss FC302 frequency converter is controlled through a dSPACE DS1006 platform using proportional resonant (PR) current controllers. The dc-link voltage is kept constant from a dc power supply (limited to 5 kW at the time of experiments). The power loss and power quality indices are measured with the N4L PPA 5530 power analyzer and they are summarized in Table IV.

An ac power source (California Instruments MX35) is used for emulating the grid in order to provide an accurate low grid side impedance (equivalent inductance of ≈0.1 mH), which is especially important for the trap filter topologies tests.
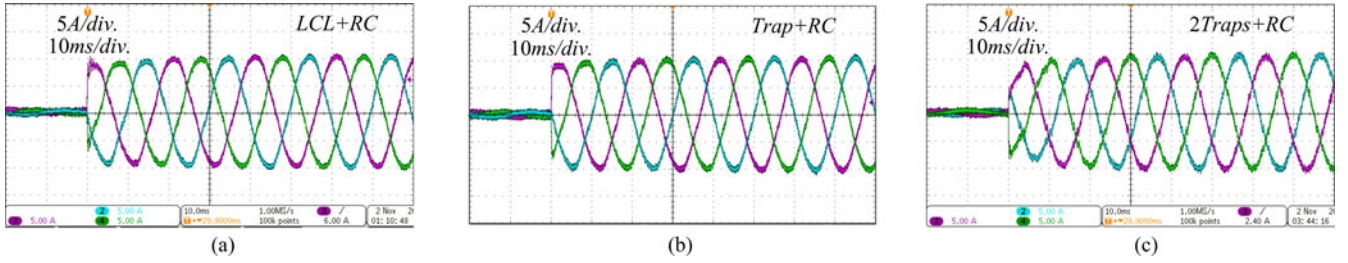
Fig. 23.   Step response from zero to half load current for: (a) *LCL* with shunt *RC* damper, (b) *Trap* and shunt *RC* damper, (c) *2Traps* and shunt *RC* damper.
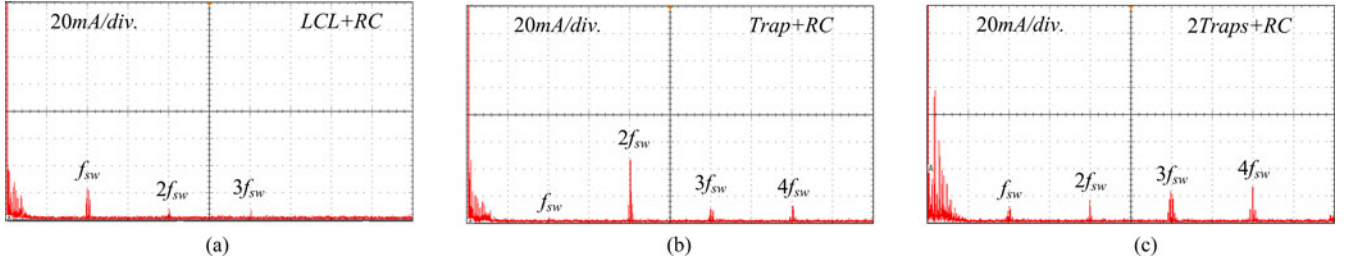

Fig. 24.   Steady-state harmonic spectrum of the grid current for: (a) *LCL* with shunt *RC* damper, (b) *Trap* with shunt *RC* damper, (c) *Two traps* with shunt *RC* damper.

B. Loss/Volume Evaluation

The passive-damped power filter prototypes are illustrated in Fig. 21. The filter volume in the case of the *LCL* with shunt *RC* damper is about 2.28 dm^3, which is around two times larger than the *two traps* filter and same damping circuit. However, for more accurate evaluation of the volume, the LI^2 factor from Table III can be used since it is proportional with the volume of the magnetic core, regardless of the adopted material. The overall filter losses are in the range of 1% for all the three built filter topologies, which is an agreement with [27] for a loss-optimized design of the overall power filter. However, the magnetic materials adopted in this design are different than in [27]; therefore, the 1% loss limit is adopted as a generic design guideline. The passive damping losses are in good agreement with the calculated damping losses illustrated in Fig. 17. The converter side inductors in Table III are designed with the nominal inductance at the peak current rating. A dc bias test of the *LCL* and *trap* filter converter side inductor is illustrated in Fig. 22. The design was made for a 30% permeability decrease as considered in the worst-case scenario in Section V-C.

C. Dynmamic Test

In Fig. 23, a dynamic test is performed with a step in the load from zero to the half the rated current. No oscillatory behavior is observed during experimental tests.

D. Harmonic Attenuation Performance

The harmonic spectrum of the grid current is illustrated in Fig. 24 with the total harmonic current distortion (THD$_{i2}$) (see Table IV) well below the 5% limit recommended in IEEE Std. 1547-2008. Since the experimental tests are conducted at half load and the filer inductance is therefore higher, the most dom-
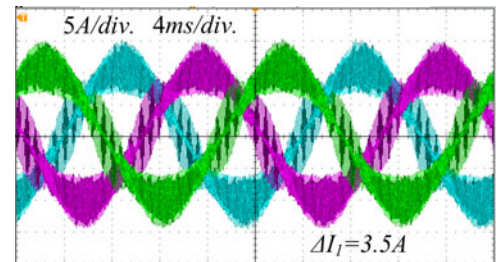

Fig. 25.   Converter current ripple at half load for the *two traps* and *RC* damping shunt filter.

inant harmonic current around the switching frequency is also well below the calculated limit illustrated in Fig. 16 (which assume ideal passive components).

E. Design Validation of the Individual Traps and the Passive Damping Circuit

The converter current ripple at half load for the *two traps* filter is around 35% and it is illustrated in Fig. 25. The rated current ripple is resulting in around 18% which is in agreement with the inductor value given in (36). The validation of the damping circuit and of the tuned traps is shown for *two traps* filter in Fig. 26.

It can be noticed that even with a very small capacitor in the second trap, the current harmonics around twice the switching frequency are successfully suppressed to the expected value. Hence, the split factor of the tuned capacitors is adequately chosen. A very low percentage total inductance is achieved for the *two traps* filter ($\approx$2%) because of the multituned traps which is around two times less than that of the *LCL* filter ($\approx$4%).
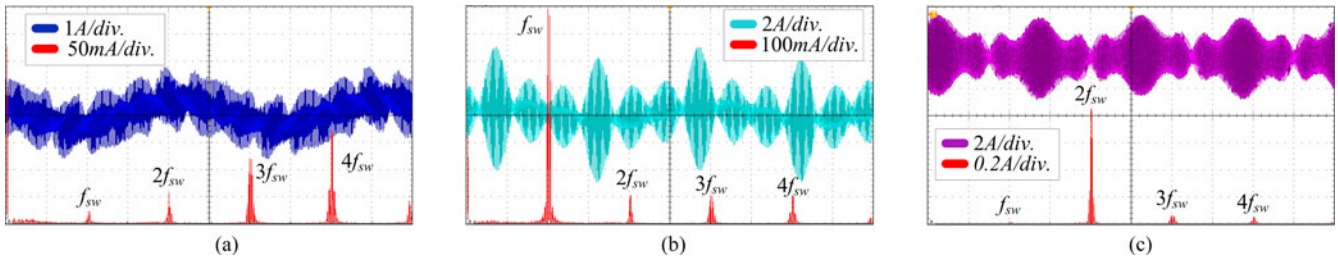
Fig. 26.   Current waveforms in the case of the *two traps* filter and shunt *RC* damper: (a) damping current, (b) first trap current, (c) second trap current.

VII. CONCLUSION

In this paper, an optimum design procedure of a shunt *RC* damper has been proposed for the *LCL* filter and multituned *traps* filter. The design method has been generalized and can be applied for any ratings of the passive filters and can be extended likewise to other passive damping methods. The method allows deriving useful expressions for the actual resonance frequency of the filter, quality factor, and the damping resistor that ensures that the peak in the filter admittance is minimal. A simple iterative design method of the overall filter has been proposed based on practical considerations which reduce the excessive trial-error procedures, related to the passive damping design of the filter. The proposed design method was validated analytically for a wide range of grid impedance variations and tested under different operating conditions of the passive components which reflect typical operating points found in low-voltage applications. In experimental tests, the size and volume of the *two trap* filter with shunt *RC* damper are obtained to about the half of the *LCL* filter with the same damping topology. One reason is a more accurate split factor design that is introduced to split the trap capacitance more efficiently depending on the harmonic limit requirement. Another advantage of the proposed method is that the ratings of the resistor can be highly reduced.

REFERENCES

[1] M. Liserre, F. Blaabjerg, and S. Hansen, "Design and control of an LCL-filter-based three-phase active rectifier," *IEEE Trans. Ind. Appl.*, vol. 41, no. 5, pp. 1281–1291, Sep. 2005.

[2] M. Prodanovic and T. C. Green, "Control and filter design of three-phase inverters for high power quality grid connection," *IEEE Trans. Power Electron.*, vol. 18, no. 1, pp. 373–380, Jan. 2003.

[3] T. C. Y. Wang, "Output filter design for a grid-interconnected three-phase inverter," in *Proc. IEEE 34th Annu. Conf. Power Electron. Spec.*, 2003, vol. 2, pp. 779–784.

[4] R. Teodorescu, F. Blaabjerg, M. Liserre, and A. Dell'Aquila, "A stable three-phase LCL-filter based active rectifier without damping," in *Proc. 38th IAS Annu. Meet. Conf. Record Industry Appl. Conf.*, 2003, vol. 3, pp. 1552–1557.

[5] B. Bolsens, K. De Brabandere, J. Van Den Keybus, J. Driesen, and R. Belmans, "Model-based generation of low distortion currents in grid-coupled PWM-inverters using an LCL output filter," *IEEE Trans. Power Electron.*, vol. 21, no. 4, pp. 1032–1040, Jul. 2006.

[6] K. K. Jalili and S. Bernet, "Design of LCL filters of active-front-end two-level voltage-source converters," *IEEE Trans. Ind. Electron.*, vol. 56, no. 5, pp. 1674–1689, May 2009.

[7] A. A. Rockhill, M. Liserre, R. Teodorescu, and P. Rodriguez, "Grid-filter design for a multimegawatt medium-voltage voltage-source inverter," *IEEE Trans. Ind. Electron.*, vol. 58, no. 4, pp. 1205–1217, Apr. 2011.

[8] Y. Patel, D. Pixler, and A. Nasiri, "Analysis and design of TRAP and LCL filters for active switching converters," in *Proc. IEEE Int. Symp. Ind. Electron.*, Jul. 2010, pp. 638–643.

[9] W. Wu, Y. He, and F. Blaabjerg, "An LLCL power filter for single-phase grid-tied inverter," *IEEE Trans. Power Electron.*, vol. 27, no. 2, pp. 782–789, Feb. 2012.

[10] J. M. Bloemink and T. C. Green, "Reducing passive filter sizes with tuned traps for distribution level power electronics," presented at the 14th Eur. Conf. Power Electron. Appl., Birmingham, U.K., 2011.

[11] S. G. Parker, B. P. McGrath, and D. G. Holmes, "Regions of active damping control for LCL filters," *IEEE Trans. Ind. Appl.*, vol. 50, no. 1, pp. 424–432, Jan. 2014.

[12] C. Zou, B. Liu, S. Duan, and R. Li, "Influence of delay on system stability and delay optimization of grid-connected inverters with LCL filter," *IEEE Trans. Ind. Inf.*, vol. 10, no. 3, pp. 1775–1784, Aug. 2014.

[13] X. Wang, F. Blaabjerg, and W. Wu, "Modeling and analysis of harmonic stability in an AC power-electronics-based power system," *IEEE Trans. Power Electron.*, vol. 29, no. 12, pp. 6421–6432, Dec. 2014.

[14] J. Sun, "Small-signal methods for AC distributed power systems—A review," *IEEE Trans. Power Electron.*, vol. 24. no. 11, pp. 2545–2554, Nov. 2009.

[15] J. Dannehl, M. Liserre, and F. W. Fuchs, "Filter-based active damping of voltage source converters with LCL filter," *IEEE Trans. Ind. Electron.*, vol. 58, no. 8, pp. 3623–3633, Aug. 2011.

[16] R. Peña-Alzola, M. Liserre, F. Blaabjerg, R. Sebastián, J. Dannehl, and F. W. Fuchs, "Analysis of the passive damping losses in LCL-filter-based grid converters," *IEEE Trans. Power Electron.*, vol. 28, no. 6, pp. 2642–2646, Jun. 2013.

[17] R. Beres, X. Wang, F. Blaabjerg, C. L. Bak, and M. Liserre, "A review of passive filters for grid-connected voltage source converters," in *Proc. IEEE Appl. Power Electron. Conf. Expo.*, 2014, pp. 2208–2215.

[18] W. Wu, Y. Sun, M. Huang, X. Wang, H. Wang, F. Blaabjerg, M. Liserre, H. S. Chung, and S. Member, "A robust passive damping method for LLCL-filter-based grid-tied inverters to minimize the effect of grid harmonic voltages," *IEEE Trans. Power Electron.*, vol. 29, no. 7, pp. 3279–3289, Jul. 2014.

[19] P. Channegowda and V. John, "Filter optimization for grid interactive voltage source inverters," *IEEE Trans. Ind. Electron.*, vol. 57, no. 12, pp. 4106–4114, Dec. 2010.

[20] R. D. Middlebrook, "Design techniques for preventing input-filter oscillations in switched-mode regulators," in *Proc. Power Convers. Conf.*, 1978, pp. A3.1–A3.16.

[21] R. W. Erickson, "Optimal single resistors damping of input filters," in *Proc. 14th Annu. Appl. Power Electron. Conf. Expo.*, 1999, pp. 1073–1079, vol. 2.

[22] J. Shi, J. Shen, Q. Chen, and S. Schröder, "Performance evaluation of current control strategies in LCL-filtered high-power converters with low pulse ratios," in *Proc. IEEE Energy Convers. Expo.*, 2014, pp. 3234–3242.

[23] W. Wu, Y. He, T. Tang, and F. Blaabjerg, "A new design method for the passive damped LCL and LLCL filter-based single-phase grid-tied inverter," *IEEE Trans. Ind. Electron.*, vol. 60, no. 10, pp. 4339–4350, Oct. 2013.

[24] G. Gohil, S. Member, L. Bede, and S. Member, "Line filter design of parallel interleaved VSCs for high power wind energy conversion systems," *IEEE Trans. Power Electron.*, vol. PP, no. 99, pp. 1-1, 2015, DOI: 10.1109/TPEL.2015.2394460.

[25] J. Xu, J. Yang, J. Ye, Z. Zhang, and A. Shen, "An LTCL filter for three-phase grid-connected converters," *IEEE Trans. Power Electron.*, vol. 29, no. 8, pp. 4322–4338, Aug. 2014.

[26] *IEEE Standard for Interconnecting Distributed Resources With Electric Power Systems*, IEEE Std 1547.2-2008, April. 2009.

[27] J. Muhlethaler, M. Schweizer, R. Blattmann, J. W. Kolar, and A. Ecklebe, "Optimal design of LCL harmonic filters for three-phase PFC rectifiers," *IEEE Trans. Power Electron.*, vol. 28, no. 7, pp. 3114–3125, Jul. 2013.

[28] S. Skogestad and I. Postlethwaite, *Multivariable Feedback Control: Analysis and Design*. Hoboken, NJ, USA: Wiley, vol. 21, 2005.

[29] Y. Tang, P. C. Loh, P. Wang, F. H. Choo, F. Gao, and F. Blaabjerg, "Generalized design of high performance shunt active power filter with output LCL filter," *IEEE Trans. Ind. Electron.*, vol. 59, no. 3, pp. 1443–1452, Mar. 2012.

[30] M. Liserre, F. Blaabjerg, and A. Dell'Aquila, "Step-by-step design procedure for a grid-connected three-phase PWM voltage source converter," *Int. J. Electron.*, vol. 91, no. 8, pp. 445–460, Aug. 2004.

Remus Narcis Beres (S'13) received the M.Sc. degrees in electrical engineering and wind power systems from Transylvania University, Brasov, Romania, and Aalborg University, Aalborg, Denmark, in 2012 and 2013, respectively. Since 2013, he has been working toward the Ph.D. degree at Aalborg University in the field of power filters.

He was with the distribution network operator Electrica Distribution South Transylvania, Brasov, Romania, from 2010 to 2011. In 2015, he was a Visiting Scholar at Tokyo Metropolitan University, Japan. His main research interests include power electronics for distributed generation, power quality, and passive components characterization.
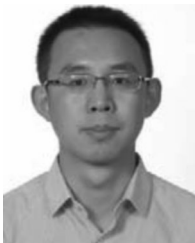
Xiongfei Wang (S'10–M'13)) received the B.Sc. degree from Yanshan University, Qinhuangdao, China, in 2006, the M.Sc. degree from Harbin Institute of Technology, Harbin, China, in 2008, both in electrical engineering, and the Ph.D. degree from Aalborg University, Aalborg, Denmark, in 2013.

Since 2009, he has been with the Aalborg University, Aalborg, Denmark, where he is currently an Assistant Professor in the Department of Energy Technology. His research interests include modeling and control of power converters, grid converters for renewable energy systems and microgrids, harmonic analysis and stability of power electronics based power systems. He is an Associate Editor of IEEE TRANSACTIONS ON INDUSTRY APPLICATIONS and served as the Guest Associate Editor of IEEE JOURNAL OF EMERGING AND SELECTED TOPICS IN POWER ELECTRONICS Special Issue on Harmonic Stability and Mitigation in Power Electronics Based Power Systems.

Frede Blaabjerg (S'86–M'88–SM'97–F'03) received the Ph.D. degree from Aalborg University, Aalborg, Denmark, in 1992.

He was with ABB-Scandia, Randers, Denmark, from 1987 to 1988. He became an Assistant Professor in 1992, an Associate Professor in 1996, and a Full Professor of power electronics and drives in 1998. His current research interests include power electronics and its applications such as in wind turbines, PV systems, reliability, harmonics, and adjustable speed drives.

Dr. Blaabjerg received 15 IEEE Prize Paper Awards, the IEEE PELS Distinguished Service Award in 2009, the EPE-PEMC Council Award in 2010, the IEEE William E. Newell Power Electronics Award 2014, and the Villum Kann Rasmussen Research Award 2014. He was an Editor-in-Chief of the IEEE TRANSACTIONS ON POWER ELECTRONICS from 2006 to 2012. He has been Distinguished Lecturer for the IEEE Power Electronics Society from 2005 to 2007 and for the IEEE Industry Applications Society from 2010 to 2011.

Marco Liserre (S'00–M'02–SM'07–F'13) received the M.Sc. and Ph.D. degrees in electrical engineering from the Bari Polytechnic, Bari, Italy, respectively, in 1998 and 2002, respectively.

He has been an Associate Professor at Bari Polytechnic and a Professor in reliable power electronics at Aalborg University, Aalborg, Denmark). He is currently a Full Professor and he holds the Chair of Power Electronics at Christian-Albrechts-University of Kiel, Kiel, Germany). He has published 168 technical papers (44 of them in international peer-reviewed journals), three chapters of a book and a book Grid Converters for Photovoltaic and Wind Power Systems (Hoboken, NJ, USA: Wiley, also translated in Chinese). His works have received more than 6000 citations.

Dr. Liserre is a Member of IAS, PELS, PES, and IES. He is an Associate Editor of the IEEE TRANSACTIONS ON INDUSTRIAL ELECTRONICS, the IEEE INDUSTRIAL ELECTRONICS MAGAZINE, the IEEE TRANSACTIONS ON INDUSTRIAL INFORMATICS, where he is currently Co-EIC, the IEEE TRANSACTIONS ON POWER ELECTRONICS, and the IEEE JOURNAL OF EMERGING AND SELECTED TOPICS IN POWER ELECTRONICS. He has been the Founder and an Editor-in-Chief of the IEEE INDUSTRIAL ELECTRONICS MAGAZINE, a Founder and the Chairman of the Technical Committee on Renewable Energy Systems, Co-Chairman of the International Symposium on Industrial Electronics (ISIE 2010), IES Vice-President responsible of the publications. He received the IES 2009 Early Career Award, the IES 2011 Anthony J. Hornfeck Service Award, the 2011 Industrial Electronics Magazine Best Paper Award, and the Third Prize paper award by the Industrial Power Converter Committee at ECCE 2012, 2012. He is Senior Member of IES AdCom. He received an ERC Consolidator Grant for an overall budget of 2 MEuro for the project "The Highly Efficient and Reliable smart Transformer (HEART), a new Heart for the Electric Distribution System."

Claus Leth Bak (SM'99) was born in Århus, Denmark, on April 13th, 1965. He received the B.Sc.(Hons.) degree in electrical power engineering in 1992 and the M.Sc. degree in electrical power engineering from the Department of Energy Technology, Aalborg University, Aalborg, Denmark, in 1994.

In 1999, he worked as an Assistant Professor at ET-AAU, where he holds a Professor position today. He has supervised 15 Ph.Ds and more than 50 M.Sc. theses. His main research areas include corona phenomena on overhead lines, power system modeling and transient simulations, underground cable transmission, power system harmonics, power system protection, and HVDC-VSC Offshore Transmission Networks. He is the author/coauthor of approximately 120 publications.

Mr. Bak worked as a Professional Engineer with Electric Power Transmission and Substations with specializations within the area of power system protection at the NV Net Transmission Company. He is a Member of Cigré C4.502, Cigré SC C4 study committee member, and Danish Cigré National Committee.